OPEN ACCESS
Fractals, Vol. 30, No. 5 (2022) 2240136 (18 pages)

DOI: 10.1142/S0218348X22401363



# CAPUTO-BASED MODEL FOR INCREASING STRAINS OF CORONAVIRUS: THEORETICAL ANALYSIS AND EXPERIMENTAL DESIGN

DUMITRU BALEANU[*,†,‡,¶] and ALI S. ALSHOMRANI[§]
[*]*Department of Mathematics*
*Cankaya University, Ankara, Turkey*
[†]*Institute of Space Sciences*
*Magurele-Bucharest, Romania*
[‡]*Department of Medical Research*
*China Medical University Hospital*
*China Medical University, Taichung, Taiwan*
[§]*Department of Mathematics*
*King Abdulaziz University*
*Jeddah, Saudi Arabia*
[¶]*dumitru@cankaya.edu.tr*

Received June 25, 2021
Accepted October 30, 2021
Published July 12, 2022

## Abstract

One of the most severe and troubling diseases these days is COVID-19 pandemic. The COVID-19 pandemic's dangerous effects are extremely rapid, and infection normally results in death within a few weeks. As a consequence, it is important to delve deeper into the complexities of this

[¶]Corresponding author.

elusive virus. In this study, we propose a Caputo-based model for increasing COVID-19 strains. The memory effect and hereditary properties of the fractional variant for the model enable us to fully comprehend the dynamics of the model's features. The existence of unique solution using the fixed-point theorem and Arzelá–Ascoli principle as well as the stability analysis of the model by means of Ulam–Hyer stability (UHS) and generalized Ulam–Hyer stability (GUHS) have been discussed. Furthermore, the parameters of the model are estimated using 3 months data points chosen from Nigeria using the nonlinear least-squares technique. The best-suited parameters and the optimized Caputo fractional-order parameter $\alpha$ are obtained by running simulations for both models. The proposed model is shown to comprehend the dynamical behavior of the virus better than the integer-order version. In addition, to shed more light on the model's characteristics, various numerical simulations are performed using an efficient numerical scheme.

*Keywords*: COVID-19 Pandemic; Caputo Operator; Existence of Solutions; Stability Analysis; Parameter Estimation; Optimized Fractional Order.



## 1. INTRODUCTION

Coronavirus disease 2019 (COVID-19) is a global pandemic disease that has spread exponentially. It has had a huge impact on people's lives, with over million reported cases and over million people killed in over countries and territories. COVID-19 is caused by the extreme acute respiratory syndrome coronavirus 2 (SARS-CoV-2) and has symptoms similar to pneumonia, such as a dry cough, fever, and, in more severe cases, breathing difficulties. Non-pharmaceutical therapies (NPIs) were suggested as a way to avoid contracting the disease. The World Health Organization (WHO) has proposed a number of non-pharmaceutical treatments (NPIs) to prevent the disease, including the use of a face mask to protect the nose and mouth, maintaining a distance of at least 2 m in public areas, frequent hand washing, using a tissue to cover the nose while sneezing, border and school closures, quarantine, isolation, and mass testing.[1–10]

The importance and power of mathematics in modeling the features of the infectious diseases have been shown many time, and the advantages of mathematical techniques have been used to deal with such phenomenon thereby reducing the number of patients dying from epidemics. Although experimental biology aims to conduct the required experiments to prove scientific theories, mathematical and theoretical biology is a science that investigates the underlying concepts of the creation and behavior of biological structures through theoretical analysis and mathematical models of living organisms.[11–16]

Fractional derivatives have become one of the most popular methods in mathematical biology, also known as theoretical biology, which uses mathematical tools to analyze biological systems. In addition, using applied mathematical methods and techniques to model biological systems with fractional derivatives has yielded significant benefits in both theoretical and applied fields. Instead of classical mathematical models, fractional mathematical models allow for a more comprehensive analysis, which is needed for the quantitative expression of disease models and better simulation of their behavior, as well as the process of predicting characteristics that may not be clearly visible with experimental data. The complexity of living systems is the primary reason why theoretical biology needs numerous fields of mathematics, new methods, and tools. The use of fractional derivative operators, especially non-local fractional derivatives, allows for a more thorough investigation of these complex systems. The majority of research areas are concerned with supercomplex processes involving extremely complex and nonlinear differential equations, and in order to better understand them, results are obtained using various forms of fractional derivatives, such as singular or non-singular kernels, and the fractional derivative that gives the best result is calculated through comparison analysis. Real-life data are required to make this determination as reliable as possible, so the derivative that behaves the most like real-life data are chosen as the derivative that produces the best result.[11–16]

Considering the global scenario on the series of waves of COVID-19, there is a need for more researches to timely and effectively curtail the spread of the disease. Thus, in this work, we extend a SEIHDR-based model[17] to investigate the dynamics of COVID-19 using an effective fractional operator, namely, Caputo fractional operator while maintaining the dimensional consistency within the Caputo model. This work is organized as follows: Model development as well as the motivation for using Caputo derivative are presented in Sec. 2. Some theoretical analyses such as existence, uniqueness and stability are presented in Sec. 3. In Sec. 4, nonlinear least-squares method is used for estimating the parameters' values for the extended Caputo model. Numerical simulations are performed in Sec. 5 to depict different dynamical features of the model. Finally, some concluding remarks are provided in Sec. 6.[18–25]

## 2. MODEL DEVELOPMENT

In order to obtain fitting results with biologically appropriate parameter values, a model of susceptible–exposed–infectious-hospitalized–recovered–dead was introduced via the classic SEIR-kind.[26–29] The fitting for the model had been done based on the deaths data to enunciate the COVID-19 scenario in some African countries with the most affected cases in order to provide guidance on the necessary NPIs that could help to curb outbreaks with far less socio-economic consequences. In traditional SEIR models, the population is categorized into four classes based on infection status, with S, E, I, and R representing susceptible, exposed, infectious, and recovered, respectively.

The authors in Ref. 17 considered two additional compartments for infected classes using the concepts of SARS-CoV-2 as in (12) and (13). These two additional classes are the hospitalized infected and dead compartments, denoted by H and D, respectively. Individuals who are susceptible will become infected after coming into contact with infected people. After the latency time, exposed individuals will progress to the infectious compartment. Individuals who are infected will be admitted to the hospitalized section, which can be mild or serious. Infectious individuals can be recovered after receiving successful treatment, or they can die from the infection and end up in the D compartment. Below is the proposed model by[17]

$$\begin{cases} S'(t) = -\dfrac{\beta S(t)I(t)}{N(t)}, \\ E'(t) = \dfrac{\beta S(t)I(t)}{N(t)} - \sigma E(t), \\ I'(t) = \sigma E(t) - \gamma I(t), \\ H'(t) = \rho\psi I(t) - \xi H(t), \\ D'(t) = \rho\xi H(t), \\ R'(t) = (1-\rho)\gamma I(t) + (1-\rho)\xi H(t), \end{cases} \tag{1}$$

with the initial conditions given by

$$S(0) \geq 0, \quad E(0) \geq 0, \quad I(0) \geq 0, \quad H(0) \geq 0, \quad D(0) \geq 0, \quad R(0) \geq 0. \tag{2}$$

After being motivated by continuous advancements of fractional calculus in various fields of applied sciences particularly the use of Caputo differential operator for mathematical modeling of epidemics, we present the Caputo variant of Eq. (1) in the form given below whereas the justification and motivation for using this fractional operator is also detailed in the forthcoming section.

$$\begin{cases} {}^{\mathrm{C}}\mathbb{D}^{\alpha}_{0,t}S(t) = \dfrac{1}{\Gamma(1-\alpha)}\displaystyle\int_0^t (t-\zeta)^{-\alpha}S'(\zeta)d\zeta \\ \qquad\qquad = -\dfrac{\beta^{\alpha}S(t)I(t)}{N(t)}, \\ {}^{\mathrm{C}}\mathbb{D}^{\alpha}_{0,t}E(t) = \dfrac{1}{\Gamma(1-\alpha)}\displaystyle\int_0^t (t-\zeta)^{-\alpha}E'(\zeta)d\zeta \\ \qquad\qquad = \dfrac{\beta^{\alpha}S(t)I(t)}{N(t)} - \sigma^{\alpha}E(t), \\ {}^{\mathrm{C}}\mathbb{D}^{\alpha}_{0,t}I(t) = \dfrac{1}{\Gamma(1-\alpha)}\displaystyle\int_0^t (t-\zeta)^{-\alpha}I'(\zeta)d\zeta \\ \qquad\qquad = \sigma^{\alpha}E(t) - \gamma^{\alpha}I(t), \\ {}^{\mathrm{C}}\mathbb{D}^{\alpha}_{0,t}H(t) = \dfrac{1}{\Gamma(1-\alpha)}\displaystyle\int_0^t (t-\zeta)^{-\alpha}H'(\zeta)d\zeta \\ \qquad\qquad = \rho\psi I(t) - \xi^{\alpha}H(t), \\ {}^{\mathrm{C}}\mathbb{D}^{\alpha}_{0,t}D(t) = \dfrac{1}{\Gamma(1-\alpha)}\displaystyle\int_0^t (t-\zeta)^{-\alpha}D'(\zeta)d\zeta \\ \qquad\qquad = \rho\xi^{\alpha}H(t), \\ {}^{\mathrm{C}}\mathbb{D}^{\alpha}_{0,t}R(t) = \dfrac{1}{\Gamma(1-\alpha)}\displaystyle\int_0^t (t-\zeta)^{-\alpha}R'(\zeta)d\zeta \\ \qquad\qquad = (1-\rho)\gamma^{\alpha}I(t) + (1-\rho)\xi^{\alpha}H(t), \end{cases} \tag{3}$$

with the initial conditions as defined in (2).

### 2.1. Motivation for Using Caputo-Based Model

The Caputo version for the model of COVID-19 (1) is being analyzed for the first time with use of real data of a large set, that is, 3 months which comprise 92 data points. After replacing first-order derivatives in the classical model represented in Eq. (1) with an arbitrary positive real order under the Caputo operator, we have achieved the fractional form of the originally proposed model of the epidemic. This replacement has a very strong justification which is explained via following points:

- Looking at the literature, one can easily verify that the well-known Riemann–Liouville integral formula is obtained from the Cauchy formula for the repeated integration wherein Riemann–Liouville merely replaced $n \in \mathbb{N}$ with $\alpha \in \mathbb{C}, Re(\alpha) > 0$ and nowadays this fractional integral formula is the cornerstone for the development of various numerical methods used for solving fractional ordinary and partial differential equations.
- In recent research studies,[30–33] the Caputo version of classical models of COVID-19 is successfully used along with the details for the existence of unique solution and stability analysis. Numerical simulations conducted therein proved importance of the Caputo version of the COVID-19 model over its classical counterpart.
- It is evident from various recently published literature works that the classical epidemiological models particularly concerning COVID-19 were not so successful in capturing complex chaotic transmission dynamics of the disease. On the other hand, the Caputo versions could not only capture such behavior but the same was verified and validated with the use of real data on the epidemic mostly found in reliable sources including WHO and experimentally published works.
- Moreover, the basic reproductive number explaining the number of average secondary infected cases produced when an infectious individual enters in a completely susceptible class gives us clear picture for the behavior of the disease under various values of biological parameters when considered with Caputo differential operator. See, for example Refs. 34 and 35 and most of the references cited therein.

## 3. THEORETICAL ANALYSIS

### 3.1. Results for Existence of Solutions

The new variant of the model in fractional sense under the non-local Caputo derivative is expressed as (3). In this portion, we use fixed-point theorems[36,37] to prove the existence and uniqueness of the suggested model's solution. Let us rewrite the proposed (3) model in the following format:

$$\begin{cases} {}^{\mathrm{C}}\mathbb{D}^{\alpha}_{0,t} S(t) = \zeta_1(t, S, E, I, H, D, R), \\ {}^{\mathrm{C}}\mathbb{D}^{\alpha}_{0,t} E(t) = \zeta_2(t, S, E, I, H, D, R), \\ {}^{\mathrm{C}}\mathbb{D}^{\alpha}_{0,t} I(t) = \zeta_3(t, S, E, I, H, D, R), \\ {}^{\mathrm{C}}\mathbb{D}^{\alpha}_{0,t} H(t) = \zeta_4(t, S, E, I, H, D, R), \\ {}^{\mathrm{C}}\mathbb{D}^{\alpha}_{0,t} D(t) = \zeta_5(t, S, E, I, H, D, R), \\ {}^{\mathrm{C}}\mathbb{D}^{\alpha}_{0,t} R(t) = \zeta_5(t, S, E, I, H, D, R), \end{cases} \tag{4}$$

with

$$\begin{cases} \zeta_1(t, S, E, I, H, D, R) = -\dfrac{\beta^{\alpha} S(t) I(t)}{N(t)}, \\ \zeta_2(t, S, E, I, H, D, R) = \dfrac{\beta^{\alpha} S(t) I(t)}{N(t)} - \sigma^{\alpha} E(t), \\ \zeta_3(t, S, E, I, H, D, R) = \sigma^{\alpha} E(t) - \gamma^{\alpha} I(t), \\ \zeta_4(t, S, E, I, H, D, R) = \alpha\psi I(t) - \xi^{\alpha} H(t), \\ \zeta_5(t, S, E, I, H, D, R) = \alpha\xi^{\alpha} H(t), \\ \zeta_6(t, S, E, I, H, D, R) \\ \qquad = (1-\alpha)\gamma^{\alpha} I(t) + (1-\alpha)\xi^{\alpha} H(t). \end{cases} \tag{5}$$

Now (3) becomes

$$\begin{cases} {}^{C}\mathcal{D}^{\alpha}_{0} \iota(t) = W(t, \iota(t)); \quad t \in J = [0, b], \\ 0 < \alpha \leq 1, \ \ \iota(0) = \iota_0 \geq 0, \end{cases} \tag{6}$$

only if

$$\begin{cases} \iota(t) = (S, E, I, H, D, R)^T, \\ \iota(0) = (S_0, E_0, I_0, H_0, D_0, R_0)^T, \\ W(t, \iota(t)) = (\zeta_i(t, S, E, I, H, D, R))^T, \\ \qquad\qquad i = 1, \ldots, 6. \end{cases} \tag{7}$$

$(\cdot)^T$ implies the transpose operation. Now (6) becomes

$$\begin{aligned}\iota(t) &= \iota_0 + \mathcal{J}_{0^+}^{\alpha} W(t, \iota(t)) \\ &= \iota_0 + \frac{1}{\Gamma(\alpha)} \int_0^t (t-\varrho)^{\alpha-1} W(\varrho, \iota(\varrho)) d\varrho. \end{aligned} \tag{8}$$

Let $\mathbb{E} = C([0,b];\mathbb{R})$ be Banach space for all the functions which are continuous from $\mathbb{R} \to [0,b]$ with the norm $\|\iota\| = \sup_{t\in J} |\iota(t)|$.

**Theorem 1.** *Let the function $W \in C([J,\mathbb{R}])$ and maps bounded subset of $J \times \mathbb{R}^5$ into compact subsets of $\mathbb{R}$. Further, there is a constant $\mathcal{L}_W > 0$ whereby $(A_1)$ $|W(t,\iota_1(t)) - W(t,\iota_2(t))| \le \mathcal{L}_W |\iota_1(t) - \iota_2(t)|$; $\forall\, t \in J$ and all $\iota_1, \iota_2 \in C([\mathcal{J},\mathbb{R}])$. Thus (8) which is equivalence to (3) has a unique solution whenever $\Omega\mathcal{L}_W < 1$, and*

$$\Omega = \frac{b^\alpha}{\Gamma(\alpha+1)}.$$

**Proof.** Considering $P : \mathbb{E} \to \mathbb{E}$ defined by

$$(P\iota)(t) = \iota_0 + \frac{1}{\Gamma(\alpha)} \int_0^t (t-\varrho)^{\alpha-1} W(\varrho, \iota(\varrho)) d\varrho. \tag{9}$$

Now, $P$ is the unique solution of (3) and is well-defined and it depicts the fixed point of $P$. Obviously, consider $\sup_{t\in J} \|W(t,0)\| = M_1$ and $\kappa \ge \|\iota_0\| + \Omega M_1$. Now, it suffices justify $P\mathbb{H}_\kappa \subset \mathbb{H}_\kappa$, and $\mathbb{H}_\kappa = \{\iota \in \mathbb{E} : \|\iota\| \le \kappa\}$, is convex and closed. Thus, each $\iota \in \mathbb{H}_\kappa$, we have

$$\begin{cases} |(P\iota)(t)| \le |\iota_0| + \dfrac{1}{\Gamma(\alpha)} \displaystyle\int_0^t (t-\varrho)^{\alpha-1} \\ \qquad\qquad \times |W(\varrho,\iota(\varrho))| d\varrho \\ \qquad \le \iota_0 + \dfrac{1}{\Gamma(\alpha)} \displaystyle\int_0^t (t-\varrho)^{\alpha-1} [|W(\varrho,\iota(\varrho)) \\ \qquad\qquad - W(\varrho,0)| + |W(\varrho,0)|] d\varrho \\ \qquad \le \iota_0 + \dfrac{(\mathcal{L}_W\kappa + M_1)}{\Gamma(\alpha)} \displaystyle\int_0^t (t-\varrho)^{\alpha-1} d\varrho \\ \qquad \le \iota_0 + \dfrac{(\mathcal{L}_W\kappa + M_1)}{\Gamma(\alpha+1)} b^\alpha \\ \qquad \le \iota_0 + \Omega(\mathcal{L}_W\kappa + M_1) \\ \qquad \le \kappa. \end{cases} \tag{10}$$

We justify the results. Further, for $\iota_1, \iota_2 \in \mathbb{E}$, one attains

$$\begin{aligned} &|(P\iota_1)(t) - (P\iota_2)(t)| \\ &\quad \le \frac{1}{\Gamma(\alpha)} \int_0^t (t-\varrho)^{\alpha-1} |W(\varrho,\iota_1(\varrho)) \\ &\qquad - W(\varrho,\iota_2(\varrho))| d\varrho \\ &\quad \le \frac{\mathcal{L}_W}{\Gamma(\alpha)} \int_0^t (t-\varrho)^{\alpha-1} |\iota_1(\varrho) - \iota_2(\varrho)| d\varrho \\ &\quad \le \Omega\mathcal{L}_W |\iota_1(t) - \iota_2(t)|, \end{aligned} \tag{11}$$

this justify that $\|(P\iota_1) - (P\iota_2)\| \le \Omega\mathcal{L}_W \|\iota_1 - \iota_2\|$. Thus, due to Banach contraction, the unique solution for (3) is reached. □

Now, we go for the existence of (3) solutions. By Krasnoselskii's fixed-point justification.

**Lemma 2.** *Let $M \ne \emptyset$ be a closed, bounded and convex subset of a Banach Space $\mathbb{E}$. Let two operators that respect the given relation be $P_1, P_2$.*

- *$P_1\iota_1 + P_2\iota_2 \in M$, provided that $\iota_1, \iota_2 \in M$;*
- *$P_1$ is compact and continuous;*
- *$P_2$ is a contraction mapping.*

*Then, there is $u \in M$ as far as $u = P_1u + P_2u$.*

**Theorem 3.** *Surmising $W : \mathcal{J} \times \mathbb{R}^5 \to \mathbb{R}$ is continuous and holds for the condition $(A_1)$. Further, let $(A_2)$ $|W(t,\iota)| \le \psi(t)$, for all $(t,\iota) \in J \times \mathbb{R}^5$ and $\psi \in C([0,b],\mathbb{R}_+)$.*

*Thus (3) has at least one solution whenever*

$$\mathcal{L}_K \|\iota_1(t_0) - \iota_2(t_0)\| < 1.$$

**Proof.** Setting $\sup_{t\in J} |\psi(t)| = \|\psi\|$ and $\eta \ge \|\iota_0\| + \Omega\|\psi\|$, we consider $\mathbf{B}_\eta = \{\iota \in \mathbb{E} : \|\iota\| \le \eta\}$. Assume $P_1,\ P_2$ operators on $\mathbf{B}_\eta$ expressed as

$$(P_1\iota)(t) = \frac{1}{\Gamma(\alpha)} \int_0^t (t-\varrho)^{\alpha-1} W(\varrho,\iota(\varrho)) d\varrho \quad t \in J,$$

and

$$(P_2\iota)(t) = \iota(t_0), \quad t \in J.$$

Now, each $\iota_1, \iota_2 \in \mathbf{B}_\eta$, gives

$$\begin{aligned} &\|(P_1\iota_1)(t) + (P_2\iota_2)(t)\| \\ &\quad \le \|\iota_0\| + \frac{1}{\Gamma(\alpha)} \int_0^t (t-\varrho)^{\alpha-1} \|W(\varrho,\iota_1(\varrho))\| d\varrho \\ &\quad \le \|\iota_0\| + \Omega\|\psi\| \\ &\quad \le \eta < \infty. \end{aligned} \tag{12}$$

Thus, $P_1\iota_1 + P_2\iota_2 \in \mathbf{B}_\eta$.

Further, the contraction of $P_2$ will be proved.

For $t \in J$ and $\iota_1, \iota_2 \in \mathbf{B}_\eta$, one reaches

$$\|(P_2\iota_1)(t) - (P_2\iota_2)(t)\| \leq \|\iota_1(t_0) - \iota_2(t_0)\|. \quad (13)$$

Having $W$ as continuous function, $P_1$ will also be continuous. Moreover, for any $t \in J$ and $\iota_1 \in \mathbf{B}_\eta$, $\|P_1\iota\| \leq \Omega\|\psi\| < +\infty$, implies that $P_1$ is uniformly bounded. Finally, one can justify that $P_1$ is compact. Define $\sup_{(t,\iota)\in J\times\mathbf{B}_\eta} |W(t,\iota(t))| = W^*$, yields

$$\begin{aligned}
&|(P_1\iota)(t_2) - (P_1\iota)(t_2)| \\
&\quad = \frac{1}{\Gamma(\alpha)}\left|\int_0^{t_1}[(t_2-\varrho)^{\alpha-1} - (t_1-\varrho)^{\alpha-1}]\right. \\
&\qquad \times W(\varrho,\iota(\varrho))d\varrho + \int_{t_1}^{t_2}(t_2-\varrho)^{\alpha-1} \\
&\qquad \left.\times W(\varrho,\iota(\varrho))d\varrho\right| \\
&\quad \leq \frac{W^*}{\Gamma(\alpha)}\left[2(t_2-t_1)^\alpha + (t_2^\alpha - t_1^\alpha)\right] \\
&\quad \to 0, \quad \text{as } t_2 \to t_1. \qquad (14)
\end{aligned}$$

This shows that by Arzelá–Ascoli principle, (3) has at least one solution. □

### 3.2. Stability Results

To prove the stability, we let $\Upsilon : X \to X$ be an operator such that it satisfies

$$\Upsilon(\iota) = \iota, \quad \iota \in X. \quad (15)$$

**Definition 4.** Equation (15) is UHS,[38,39] if for $\urcorner > 0$ and let $\iota \in \Upsilon$ be any solution of the inequality given by

$$\|\iota - \Upsilon\iota\| \leq \urcorner, \quad \forall\, t \in [0,T], \quad (16)$$

there exists one and only one solution $\bar{\iota}$ for Eq. (15) with the occurrence of a constant $C_q > 0$ and satisfy

$$\|\bar{\iota} - \iota\| \leq C_q\urcorner, \quad \forall\, t \in [0,T]. \quad (17)$$

**Definition 5.** If $\exists\, \theta \in C(R,R)$ with $\theta(0) = 0$, for one and only one solution $\bar{\iota}$ and any solution of Eq. (15) such that

$$\|\bar{\iota} - \iota\| \leq \theta(\urcorner), \quad (18)$$

then Eq. (15) is GUHS.

**Remark 6.** If $\exists\, \hbar(t) \in C([0,T],R)$, then $\bar{\iota} \in X$ satisfy (16) if

(i) $|\hbar(t)| \leq \urcorner$, $\forall\, t \in [0,T]$,
(ii) $\Upsilon\bar{\iota}(t) = \bar{\iota} + \hbar(t)$, $\forall\, t \in [0,T]$.

We need the following relation for further proofs. Here we consider a perturbed equation of the perturbed problem (4) as

$$\begin{cases} {}^C\mathcal{D}_0^\alpha\iota(t) = W(t,\iota(t)) + \hbar(t), \\ \iota(0) = \iota_0. \end{cases} \quad (19)$$

**Lemma 7.** *The result mentioned below holds for Eq.* (20)

$$|\iota(t) - \digamma\iota(t)| \leq a\urcorner, \quad \textit{where } a = \frac{T^\alpha}{\Gamma(\alpha+1)}. \quad (20)$$

**Theorem 8.** *By Lemma* 7, *the solution of the presented problem in this paper* (4) *is UHS and also GUHS, if* $\frac{T^\alpha L_\omega}{\Gamma(\alpha+1)} < 1$.

**Proof.** Let $\iota \in X$ be any result and $\bar{\iota} \in X$ be the unique result of Eq. (4), then

$$\begin{aligned}
|\iota(t) - \bar{\iota}(t)| &= |\iota(t) - \digamma\bar{\iota}(t)|, \\
&\leq |\iota(t) - \digamma\iota(t)| + |\digamma\iota(t) + \digamma\bar{\iota}(t)|, \\
&\leq a\urcorner + \frac{T^\alpha L_\phi}{\Gamma(\alpha+1)}|\iota(t) - \bar{\iota}(t)|, \\
&\leq \frac{a\urcorner}{1 - \frac{T^p L_\theta}{\Gamma(\alpha+1)}}. \qquad (21)
\end{aligned}$$

which clarifies that the studied problem (4) is UHS, also it is GUHS, by considering

$$Y(\urcorner) = \frac{a\urcorner}{1 - \frac{T^\alpha L_\theta}{\Gamma(\alpha+1)}}. \quad (22)$$

$\ni Y(0) = 0$. □

**Definition 9.** Equation (15) is UHS for $g \in C([0,T],R)$, if for $\epsilon > 0$ and let $\iota \in X$ be any result of the following inequality:

$$\|\iota - H\iota\| \leq g(t)\urcorner, \quad (23)$$

$\exists$ one and only one solution $\bar{\iota}$ for (15) with the additional condition of $K_q > 0 \ni$

$$\|\bar{\iota} - \iota\| \leq K_q g(t)\urcorner, \quad \forall\, t \in [0,T]. \quad (24)$$

**Definition 10.** For $g \in C[[0,T],R]$, if $\exists\, K_{q,g}$ and for $\urcorner > 0$, we assume that $\iota$ be a unique result of (24) and $\bar{\iota}$ be any other solution other than the unique solution of (15) $\ni$

$$\|\bar{\iota} - \iota\| \leq K_{q,g}g(t), \quad \forall\, t \in [0,T], \quad (25)$$

after these holds, Eq. (15) is GUHS.

**Remark 11.** If $\exists\, \hbar(t) \in C([0,T],R)$, then $\bar{\iota} \in X$ satisfies (16), if

(i) $|\hbar(t)| \leq (t)$, $\forall\, t \in [0,T]$,
(ii) $\Upsilon\bar{\iota}(t) = \bar{\iota} + \hbar(t)$, $\forall\, t \in [0,T]$.

**Lemma 12.** *Equation* (20) *holds the result stated below*

$$|\iota(t) - \digamma\,\iota(t)| \leq ag(t)\urcorner, \quad \textit{where } a = \frac{T^{\alpha}}{\Gamma(\alpha+1)}. \tag{26}$$

**Proof.** The proof is easy. □

**Theorem 13.** *By Lemma* 4.9, *the result of the studied problem* (4) *is UHS & GUHS also, if* $\frac{T^{\alpha}L_{\phi}}{\Gamma\alpha+1} < 1$.

**Proof.** Let $\iota \in X$ be any other solution than the unique solution and $\bar{\iota} \in X$ be the unique result for Eq. (4) then

$$\begin{aligned}
|\iota(t) - \bar{\iota}(t)| &= |\iota(t) - \digamma\,\bar{\iota}(t)|,\\
&\leq |\iota(t) - \digamma\,\iota(t)| + |\digamma\,\iota(t) + \digamma\,\bar{\iota}(t)|,\\
&\leq a \cdot g(t)\urcorner + \frac{T^{\alpha}L_{\phi}}{\Gamma(\alpha+1)}|\iota(t) - \bar{\iota}(t)|,\\
&\leq \frac{a.g(t)\urcorner}{1 - \frac{T^{\alpha}L_{\theta}}{\Gamma(\alpha+1)}}.
\end{aligned} \tag{27}$$

Therefore, Eq. (4) is UHS, and also GUHS. □

## 4. NONLINEAR LEAST-SQUARES METHOD FOR BIOLOGICAL PARAMETERS

It is well known that various mathematical models having different characteristics can be designed to explain dynamics of an epidemic. To value a model over the others, some statistics can be performed. After an epidemiological model is finalized, next comes its validation which means that it has to be compared with the available real data for the infectious individuals on daily, weekly, monthly or yearly basis. This type of task is considered to be one of the challenging tasks during the construction of the well-established model.

The validation process of the model indeed provides the degree to which the designed model shows an accurate representation of the real-world data. In most of the research papers on epidemiological modeling, validation is often neglected due to non-availability of real data or its inaccuracies. On the other hand, linking the epidemiological model to real data is essential, for it assists one to not only create more confidence in the designed model, but also to achieve realistic estimates of the biological parameters the model depends on.

Moreover, when an explicit or implicit solution of the epidemiological models is accessible then fitting data to such solutions of the model is in fact not a big deal. However, this is not the case in most of the models we encounter and this is due to nonlinear terms in the model and thus no explicit solution exists. Availability of real data varies as it could be given to us in the form of either infectious cases, or recovered ones or even those hospitalized but it is mostly given in the time series format. One of the commonly used approaches for fitting the data is the approach called the nonlinear least-squares approach. It is this approach we have utilized in this section to fit the real COVID-19 daily cases from 1 November 2020 to 31 January 2021, in Nigeria. This time period (3 months) contains, in total, 92 data points for infectious compartment in the model both in classical (1) and the Caputo sense (3).

In this study, it is worth to be noted that such a large dataset has rarely been fitted via Caputo operator in the existing literature for epidemiological modeling of COVID-19 for any country so far. By reducing the residuals, the objective function has been simulated until the most minimum residue is achieved via MATLAB differential equations solver known as *ode23*, minimization routine *fminsearch* and few more necessary built-in commands. By running the simulations of both models, we have achieved best-fitted parameters that are listed in Table 1 noting that along with the biological parameters we have also been able to receive the optimized Caputo fractional-order parameter $\alpha$ to be approximately equal to $9.6481e-01$ whereas the minimum in the classical and the Caputo sense is obtained as $4.1543e+02$ and $4.0109e+02$, respectively, noting that the Caputo results in smaller error. All real cases of COVID-19 on daily basis within the chosen time period have been reported in Table 3 including those predicted values obtained via classical and the Caputo operator. Similarly, absolute errors computed under both situations are also tabulated within Table 4 while observing that smaller errors come with the Caputo operator. The basic reproductive number in the Caputo sense is also better than the classical one taking, respectively, the values $3.0472e+00$ and $2.1895e+00$. Thus, it shows that assuming biological parameters in the Caputo sense and simulating the fractional

**Table 1 Best-Fitted Parameters for Classical ($\alpha = 1$) and Caputo ($\alpha \neq 1$) Version of the COVID Model.**

| Parameters | Interpretation | $\alpha = 1$ | $\alpha \neq 1$ |
|---|---|---|---|
| $\beta$ | transmission rate | 6.8412e-01 | 6.8412e-01 |
| $\sigma$ | progression rate of the disease from latent to infection's stage | 2.5591e-02 | 4.3974e-02 |
| $\gamma$ | recovery or hospitalization rate | 2.2451e-01 | 3.1245e-01 |
| $\xi$ | disease induced death rate | 5.9895e-01 | 6.9370e-01 |
| $\rho$ | proportion of hospitalization and death | 2.2623e-03 | 3.3405e-03 |
| $\psi$ | over-dispersion parameter | 2.9233e-03 | 1.7353e-03 |
| $\alpha$ | fractional-order parameter | 1.0000e-00 | 9.6481e-01 |

**Table 2 Summary Statistics for the Real COVID-19 Daily Cases, Classical Simulations and Simulations under the Caputo Operator.**

| Data | Min. | First Qu. | Median | Mean | Third Qu. | Max. |
|---|---|---|---|---|---|---|
| Real | 0 | 1.5950e + 02 | 4.8750e + 02 | 7.3767e + 02 | 1.2855e + 03 | 2.6090e + 03 |
| Classical | 1.0496e + 02 | 1.6708e + 02 | 3.9884e + 02 | 6.3763e + 02 | 9.5338e + 02 | 2.2359e + 03 |
| Caputo | 1.1590e + 02 | 1.9632e + 02 | 4.4144e + 02 | 6.6251e + 02 | 9.9078e + 02 | 2.1827e + 03 |

model are alternatively better options. Figures 1 and 2 represent dynamical behavior of the infectious compartment and their best fitting with the time series data for the real COVID-19 cases under both classical and the Caputo operator with their respective residuals.

With close examination, it can be observed that the real COVID-19 daily cases are best fitted under the Caputo simulations with smaller possible residuals. In addition, some statistical parameters are included for further comparison such as the box plot in Fig. 3 wherein two outliers are found in the classical case whereas only one outlier is observed in the Caputo simulations with optimized fractional-order parameter. Included are statistical measures in Table 2 which show minimum, first quartile, median, mean, third quartile and the maximum values in the real daily cases of COVID-19, classical and the Caputo simulations in the first, second and the third row; respectively. The table shows most of the statistics obtained under the Caputo approach are in good agreement with the real data.

## 5. NUMERICAL ASPECTS

In this section, numerical dynamics for the COVID-19 epidemic as modeled with the Caputo fractional operator have been analyzed keeping in mind that the fractional-order parameter used for simulations is the one optimized in Sec. 4 whereas rest of the parameters are taken from the last column of Table 1. An explicit predictor–corrector type of numerical method especially designed for simulations of fractional Caputo type of ordinary differential equations is employed herein. The method itself and its full analysis based upon convergence and error bounds are found in Refs. 40 and 41. The numerical method designed for this purpose has received much admiration in this literature due to its simplicity and versatility that can be seen in Refs. 42–47. The author in Ref. 48 has also discussed in detail about MATLAB implementation of the numerical method with predictor–corrector features. Use of such available routines on MathWorks made the simulations much handy for this research study for the Caputo COVID-19 model (3). It may be noted that we use MATLAB software with version '9.8.0.1323502 (R2020a)' running on OS Windows with Intel(R) Core(TM) i7-1065G7 CPU @ 1.30 GHz 1.50 GHz processor and 24 GB installed RAM.

For the chosen COVID-19 model under the Caputo operator, there are many important parameters that require attention to be observed for their values for increasing or decreasing manner. In this regard, we have chosen some parameters such as transmission rate $\beta$, recovery (or hospitalization) rate $\gamma$, progression rate of the disease from latent to infection's stage $\sigma$, and the Caputo fractional-order

**Table 3 Real COVID Cases (Row 1), Classical Simulations (Row 2), and the Caputo Simulations (Row 3).**

| | | | | | | | | | |
|---|---|---|---|---|---|---|---|---|---|
| 162 | 111 | 72 | 137 | 155 | 180 | 223 | 59 | 300 | 94 |
| 1.6200e + 02 | 1.4205e + 02 | 1.2788e + 02 | 1.1808e + 02 | 1.1159e + 02 | 1.0761e + 02 | 1.0555e + 02 | 1.0496e + 02 | 1.0552e + 02 | 1.0697e + 02 |
| 1.6200e + 02 | 1.3977e + 02 | 1.2719e + 02 | 1.2022e + 02 | 1.1686e + 02 | 1.1590e + 02 | 1.1657e + 02 | 1.1837e + 02 | 1.2099e + 02 | 1.2421e + 02 |
| 152 | 180 | 212 | 156 | 112 | 152 | 157 | 152 | 236 | 146 |
| 1.0914e + 02 | 1.1187e + 02 | 1.1508e + 02 | 1.1869e + 02 | 1.2264e + 02 | 1.2691e + 02 | 1.3145e + 02 | 1.3625e + 02 | 1.4131e + 02 | 1.4661e + 02 |
| 1.2789e + 02 | 1.3194e + 02 | 1.3630e + 02 | 1.4092e + 02 | 1.4580e + 02 | 1.5090e + 02 | 1.5623e + 02 | 1.6178e + 02 | 1.6754e + 02 | 1.7353e + 02 |
| 143 | 246 | 155 | 56 | 168 | 198 | 169 | 246 | 110 | 82 |
| 1.5215e + 02 | 1.5793e + 02 | 1.6395e + 02 | 1.7022e + 02 | 1.7675e + 02 | 1.8353e + 02 | 1.9059e + 02 | 1.9792e + 02 | 2.0554e + 02 | 2.1345e + 02 |
| 1.7974e + 02 | 1.8618e + 02 | 1.9286e + 02 | 1.9978e + 02 | 2.0695e + 02 | 2.1438e + 02 | 2.2207e + 02 | 2.3005e + 02 | 2.3830e + 02 | 2.4686e + 02 |
| 145 | 281 | 122 | 343 | 324 | 310 | 318 | 390 | 550 | 474 |
| 2.2168e + 02 | 2.3019e + 02 | 2.3908e + 02 | 2.4832e + 02 | 2.5793e + 02 | 2.6791e + 02 | 2.7825e + 02 | 2.8895e + 02 | 3.0009e + 02 | 3.1170e + 02 |
| 2.5571e + 02 | 2.6489e + 02 | 2.7439e + 02 | 2.8424e + 02 | 2.9443e + 02 | 3.0499e + 02 | 3.1592e + 02 | 3.2725e + 02 | 3.3898e + 02 | 3.5113e + 02 |
| 675 | 796 | 617 | 418 | 199 | 758 | 930 | 1145 | 806 | 920 |
| 3.2377e + 02 | 3.3630e + 02 | 3.4929e + 02 | 3.6272e + 02 | 3.7670e + 02 | 3.9126e + 02 | 4.0641e + 02 | 4.2214e + 02 | 4.3846e + 02 | 4.5533e + 02 |
| 3.6371e + 02 | 3.7674e + 02 | 3.9024e + 02 | 4.0421e + 02 | 4.1869e + 02 | 4.3368e + 02 | 4.4921e + 02 | 4.6530e + 02 | 4.8195e + 02 | 4.9920e + 02 |
| 501 | 356 | 999 | 1133 | 0 | 1825 | 829 | 838 | 397 | 749 |
| 4.7287e + 02 | 4.9114e + 02 | 5.1015e + 02 | 5.2990e + 02 | 5.5039e + 02 | 5.7159e + 02 | 5.9358e + 02 | 6.1651e + 02 | 6.4037e + 02 | 6.6516e + 02 |
| 5.1707e + 02 | 5.3558e + 02 | 5.5474e + 02 | 5.7459e + 02 | 5.9515e + 02 | 6.1645e + 02 | 6.3850e + 02 | 6.6134e + 02 | 6.8499e + 02 | 7.0950e + 02 |
| 1016 | 934 | 0 | 1653 | 917 | 1204 | 1421 | 1664 | 1565 | 1544 |
| 6.9089e + 02 | 7.1755e + 02 | 7.4512e + 02 | 7.7388e + 02 | 8.0382e + 02 | 8.3494e + 02 | 8.6724e + 02 | 9.0073e + 02 | 9.3535e + 02 | 9.7142e + 02 |
| 7.3487e + 02 | 7.6115e + 02 | 7.8837e + 02 | 8.1656e + 02 | 8.4576e + 02 | 8.7600e + 02 | 9.0732e + 02 | 9.3976e + 02 | 9.7336e + 02 | 1.0082e + 03 |
| 0 | 2609 | 1244 | 1270 | 1398 | 1479 | 1867 | 1598 | 1444 | 1617 |
| 1.0090e + 03 | 1.0480e + 03 | 1.0886e + 03 | 1.1307e + 03 | 1.1741e + 03 | 1.2194e + 03 | 1.2665e + 03 | 1.3155e + 03 | 1.3665e + 03 | 1.4193e + 03 |
| 1.0442e + 03 | 1.0815e + 03 | 1.1202e + 03 | 1.1602e + 03 | 1.2017e + 03 | 1.2446e + 03 | 1.2891e + 03 | 1.3352e + 03 | 1.3829e + 03 | 1.4323e + 03 |
| 1301 | 1386 | 1962 | 1485 | 2464 | 964 | 1430 | 1303 | 1861 | 864 |
| 1.4739e + 03 | 1.5306e + 03 | 1.5898e + 03 | 1.6513e + 03 | 1.7152e + 03 | 1.7815e + 03 | 1.8502e + 03 | 1.9214e + 03 | 1.9956e + 03 | 2.0728e + 03 |
| 1.4835e + 03 | 1.5365e + 03 | 1.5914e + 03 | 1.6483e + 03 | 1.7072e + 03 | 1.7682e + 03 | 1.8313e + 03 | 1.8968e + 03 | 1.9645e + 03 | 2.0347e + 03 |
| 1650 | 1883 | | | | | | | | |
| 2.1528e + 03 | 2.2359e + 03 | | | | | | | | |
| 2.1074e + 03 | 2.1827e + 03 | | | | | | | | |

**Table 4 Absolute Errors in the Classical Case (Row 1), and the Absolute Errors in the Caputo Case (Row 2).**

| | | | | | | | | | |
|---|---|---|---|---|---|---|---|---|---|
| 0 | 3.1045e + 01 | 5.5876e + 01 | 1.8923e + 01 | 4.3415e + 01 | 7.2391e + 01 | 1.1745e + 02 | 4.5965e + 01 | 1.9448e + 02 | 1.2973e + 01 |
| 0 | 2.8766e + 01 | 5.5185e + 01 | 1.6784e + 01 | 3.8141e + 01 | 6.4102e + 01 | 1.0643e + 02 | 5.9373e + 01 | 1.7901e + 02 | 3.0208e + 01 |
| 4.2864e + 01 | 6.8128e + 01 | 9.6919e + 01 | 3.7310e + 01 | 1.0644e + 01 | 2.5094e + 01 | 2.5552e + 01 | 1.5747e + 01 | 9.4692e + 01 | 6.0676e-01 |
| 2.4112e + 01 | 4.8063e + 01 | 7.5704e + 01 | 1.5076e + 01 | 3.3799e + 01 | 1.0963e + 00 | 7.6854e-01 | 9.7782e + 00 | 6.8456e + 01 | 2.7530e + 01 |
| 9.1465e + 00 | 8.8073e + 01 | 8.9513e + 00 | 1.1422e + 02 | 8.7484e + 00 | 1.4465e + 01 | 2.1588e + 01 | 4.8080e + 01 | 9.5536e + 01 | 1.3145e + 02 |
| 3.6742e + 01 | 5.9817e + 01 | 3.7860e + 01 | 1.4378e + 02 | 3.8950e + 01 | 1.6378e + 01 | 5.3074e + 01 | 1.5955e + 01 | 1.2830e + 02 | 1.6486e + 02 |
| 7.6679e + 01 | 5.0806e + 01 | 1.1708e + 02 | 9.4679e + 01 | 6.6067e + 01 | 4.2089e + 01 | 3.9745e + 01 | 1.0105e + 02 | 2.4991e + 02 | 1.6230e + 02 |
| 1.1071e + 02 | 1.6110e + 01 | 1.5239e + 02 | 5.8764e + 01 | 2.9570e + 01 | 5.0122e + 00 | 2.0771e + 00 | 6.2752e + 01 | 2.1102e + 02 | 1.2287e + 02 |
| 3.5123e + 02 | 4.5970e + 02 | 2.6771e + 02 | 5.5278e + 01 | 1.7770e + 02 | 3.6674e + 02 | 5.2359e + 02 | 7.2286e + 02 | 3.6754e + 02 | 4.6467e + 02 |
| 3.1129e + 02 | 4.1926e + 02 | 2.2676e + 02 | 1.3787e + 01 | 2.1969e + 02 | 3.2432e + 02 | 4.8079e + 02 | 6.7970e + 02 | 3.2405e + 02 | 4.2080e + 02 |
| 2.8134e + 01 | 1.3514e + 02 | 4.8885e + 02 | 6.0310e + 02 | 5.5039e + 02 | 1.2534e + 03 | 2.3542e + 02 | 2.2149e + 02 | 2.4337e + 02 | 8.3842e + 01 |
| 1.6072e + 01 | 1.7958e + 02 | 4.4426e + 02 | 5.5841e + 02 | 5.9515e + 02 | 1.2086e + 03 | 1.9050e + 02 | 1.7666e + 02 | 2.8799e + 02 | 3.9505e + 01 |
| 3.2511e + 02 | 2.1645e + 02 | 7.4512e + 02 | 8.7912e + 02 | 1.1318e + 02 | 3.6906e + 02 | 5.5376e + 02 | 7.6327e + 02 | 6.2965e + 02 | 5.7258e + 02 |
| 2.8113e + 02 | 1.7285e + 02 | 7.8837e + 02 | 8.3644e + 02 | 7.1240e + 01 | 3.2800e + 02 | 5.1368e + 02 | 7.2424e + 02 | 5.9164e + 02 | 5.3585e + 02 |
| 1.0090e + 03 | 1.5610e + 03 | 1.5539e + 02 | 1.3934e + 02 | 2.2386e + 02 | 2.5962e + 02 | 6.0048e + 02 | 2.8246e + 02 | 7.7536e + 01 | 1.9772e + 02 |
| 1.0442e + 03 | 1.5275e + 03 | 1.2383e + 02 | 1.0979e + 02 | 1.9632e + 02 | 2.3437e + 02 | 5.7789e + 02 | 2.6282e + 02 | 6.1104e + 01 | 1.8469e + 02 |
| 1.7290e + 02 | 1.4464e + 02 | 3.7223e + 02 | 1.6630e + 02 | 7.4878e + 02 | 8.1754e + 02 | 4.2021e + 02 | 6.1844e + 02 | 1.3462e + 02 | 1.2088e + 03 |
| 1.8250e + 02 | 1.5051e + 02 | 3.7059e + 02 | 1.6327e + 02 | 7.5683e + 02 | 8.0416e + 02 | 4.0134e + 02 | 5.9377e + 02 | 1.0353e + 02 | 1.1707e + 03 |
| 5.0284e + 02 | 3.5289e + 02 | | | | | | | | |
| 4.5741e + 02 | 2.9969e + 02 | | | | | | | | |

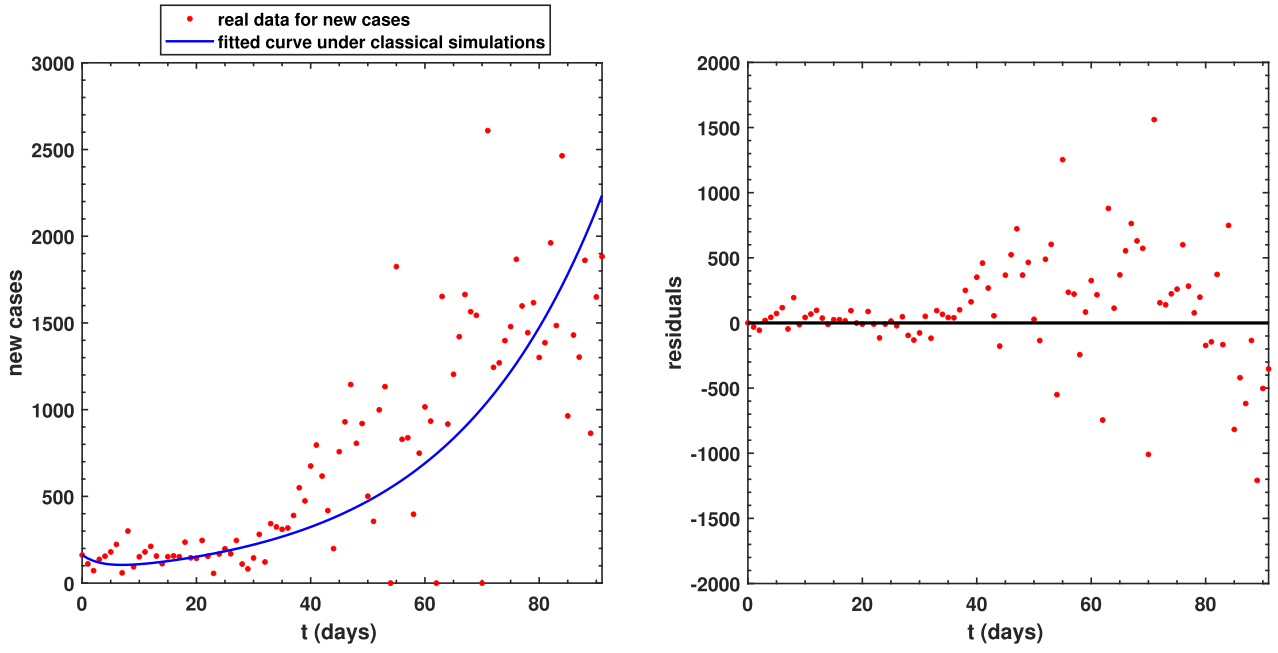


(a) (b)

**Fig. 1** **(a)** Real COVID-19 daily cases versus simulations under the class differential operator for infected individuals and their **(b)** respective residuals.

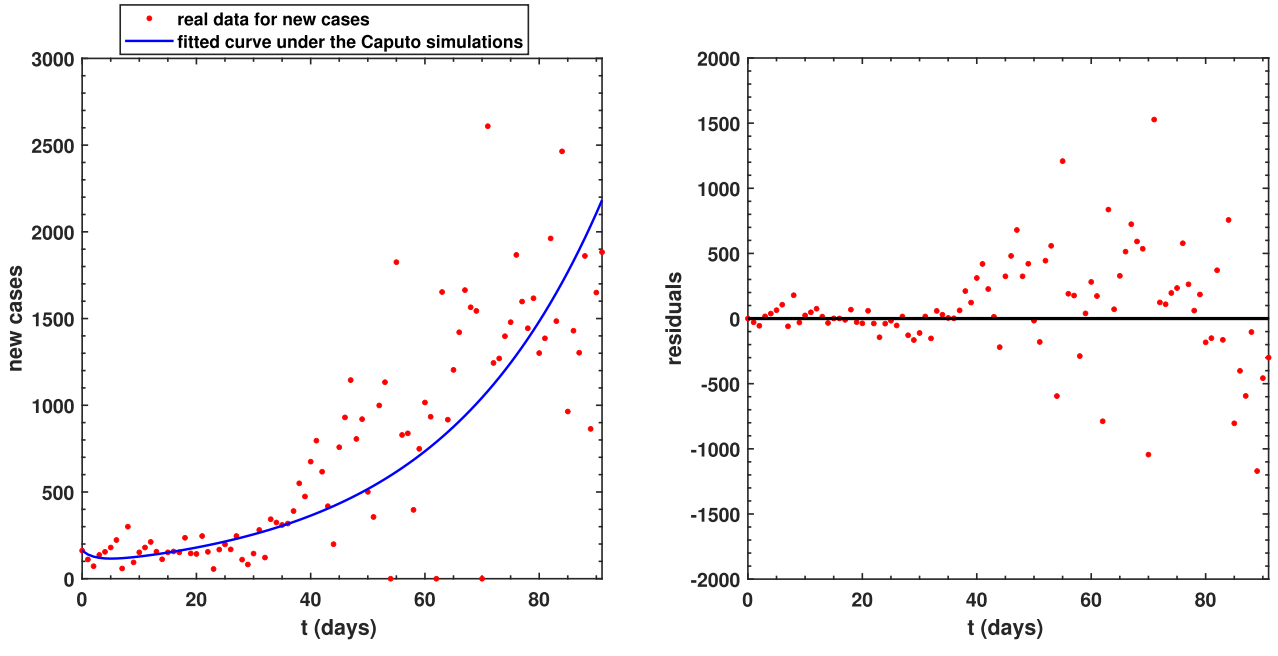


(a) (b)

**Fig. 2** **(a)** Real COVID-19 daily cases versus simulations under the Caputo differential operator for infected individuals and their **(b)** respective residuals.

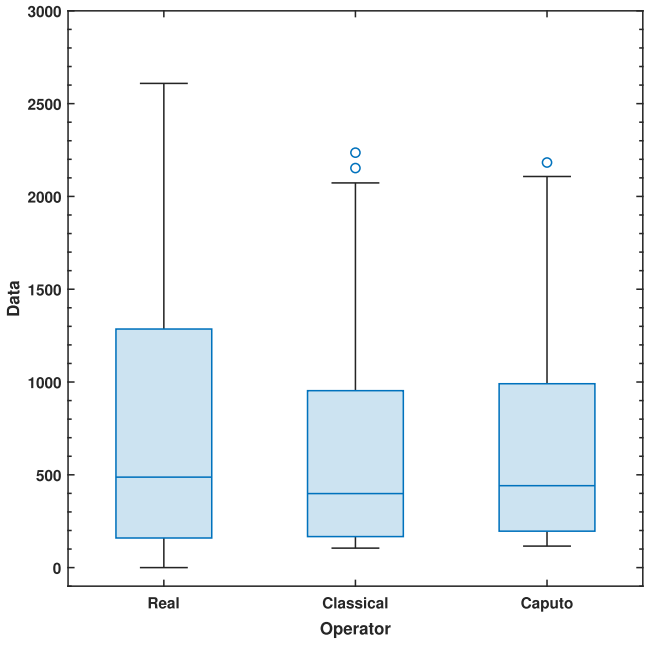


**Fig. 3** Box and Whisker plots for real data, simulations with classical and Caputo differential operator.

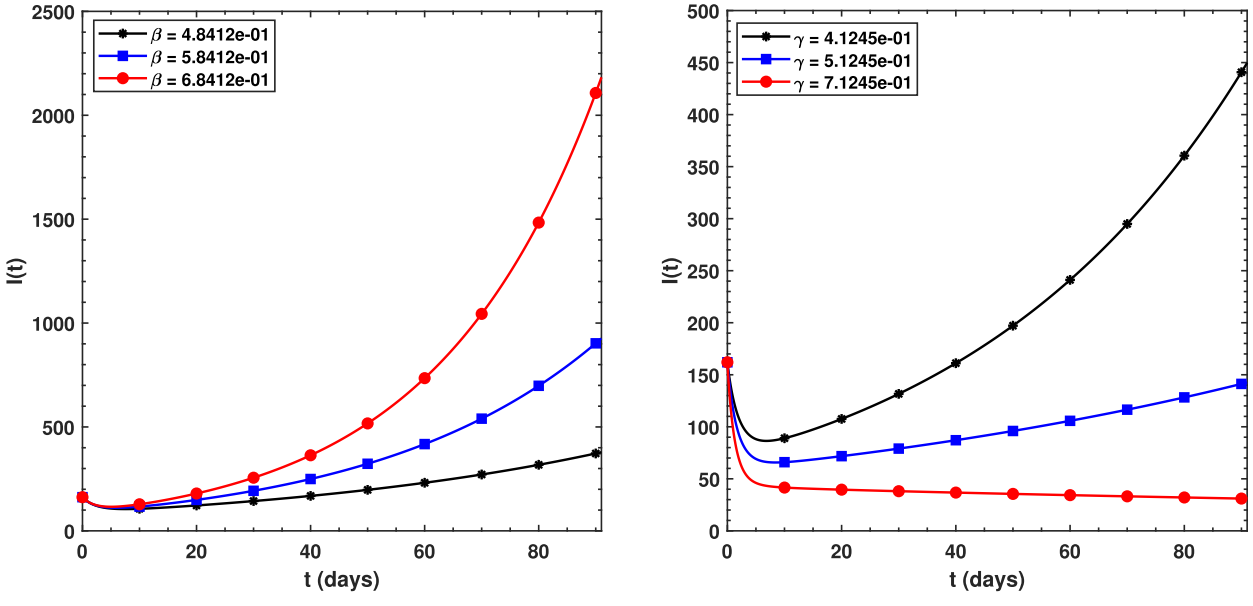


(a) (b)

**Fig. 4** **(a)** Behavior of infectious individuals for increasing transmission rate $\beta$ and **(b)** for increasing recovery rate $\gamma$.

optimized parameter $\alpha$. In addition, we have also shown numerical dynamics of all of the six state variables under the fitted parameters and the optimized value of $\alpha$ with the Caputo operator.

It is seen in Fig. 4 that for increasing value of $\beta$, although slightly, causes the infection to grow by large amount whereas for the increasing rate of recovery $\gamma$, we observe that the infectious population starts to decline. Such kind of behavior depicts the theoretical observations as well. Thus, the Caputo operator has been successful to capture the real time natural phenomenon of the epidemic. Moreover, (a) plot of Fig. 5 shows that a slight increase in the disease's progression rate from latent

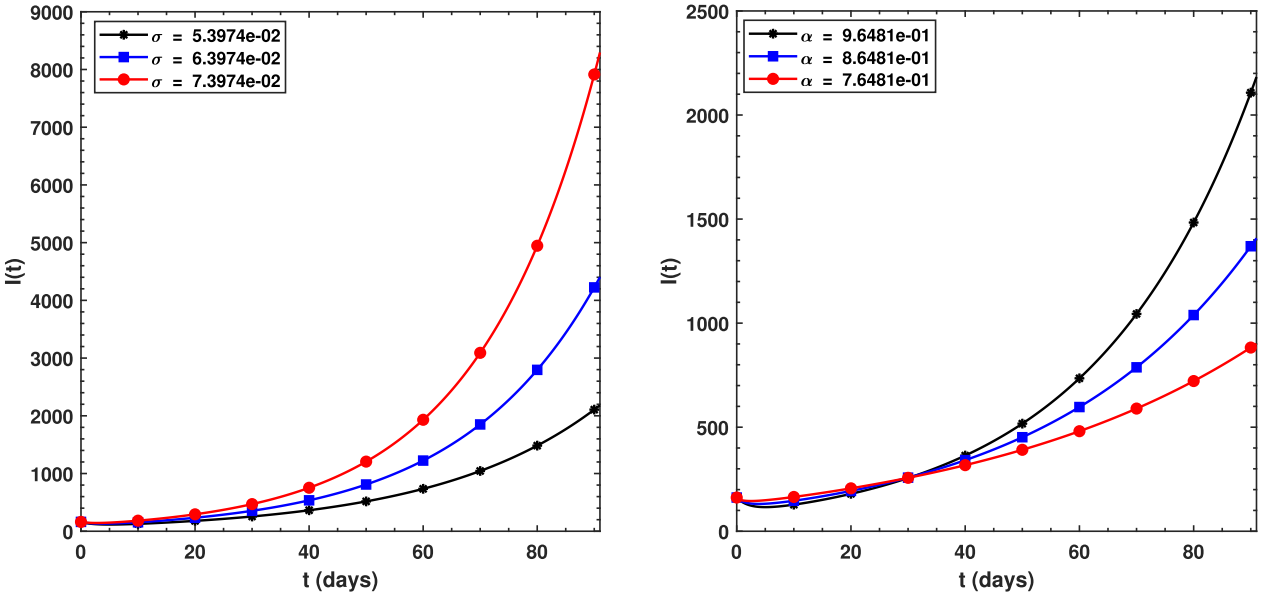


(a) (b)

**Fig. 5** **(a)** Behavior of infectious individuals for increasing progression rate $\sigma$ and **(b)** for decreasing fractional-order parameter $\alpha$.

to infection's stage brings the infectious individuals to upper position which is also the real phenomena as observed experimentally for the ongoing epidemic whereas looking the behavior of infectious class in (b) plot of this figure, it is easy to be convinced that a value $\alpha \in (0, 1)$ would be the most suitable value to capture the dynamics of the epidemic and such a value has been successfully determined in this study as equal to $\approx 9.6481e-01$. Thus, the Caputo fractional-order parameter $\alpha$ plays a vital role in transmission dynamics of the epidemic.

Finally, we carried out the simulations for each state variable in Figs. 6 to 11 under the Caputo operator for the fractional model (3). This

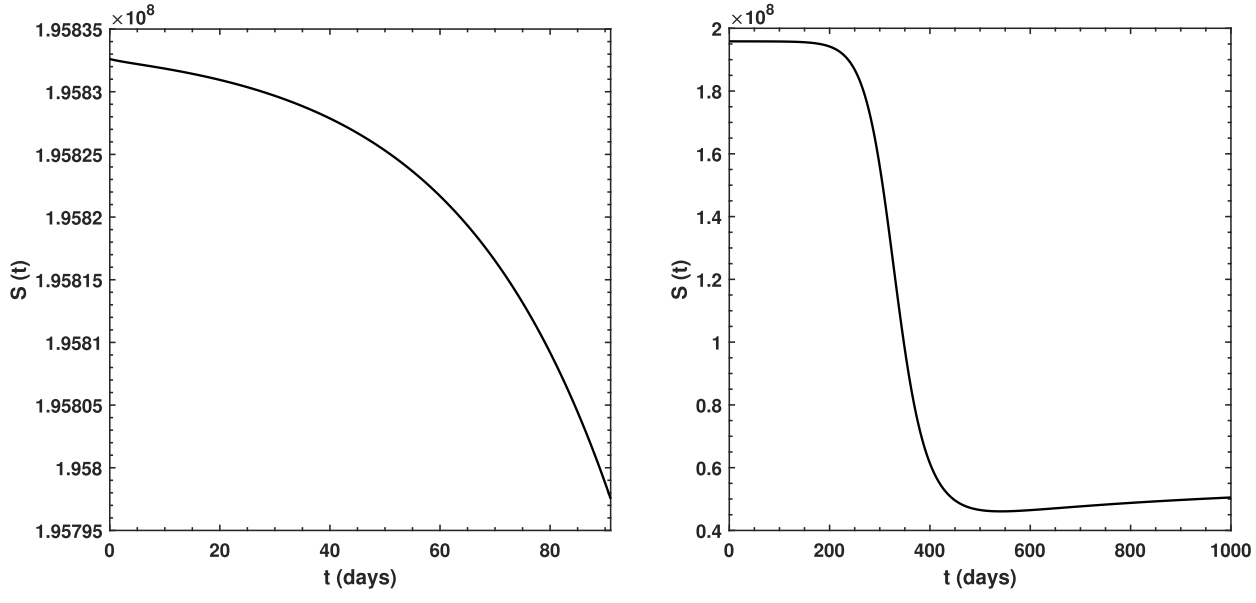


(a) (b)

**Fig. 6** **(a)** Behavior of susceptible individuals for the time period $[0, 91]$ and **(b)** behavior of susceptible individuals for the time period $[0, 1000]$ under the Caputo operator.

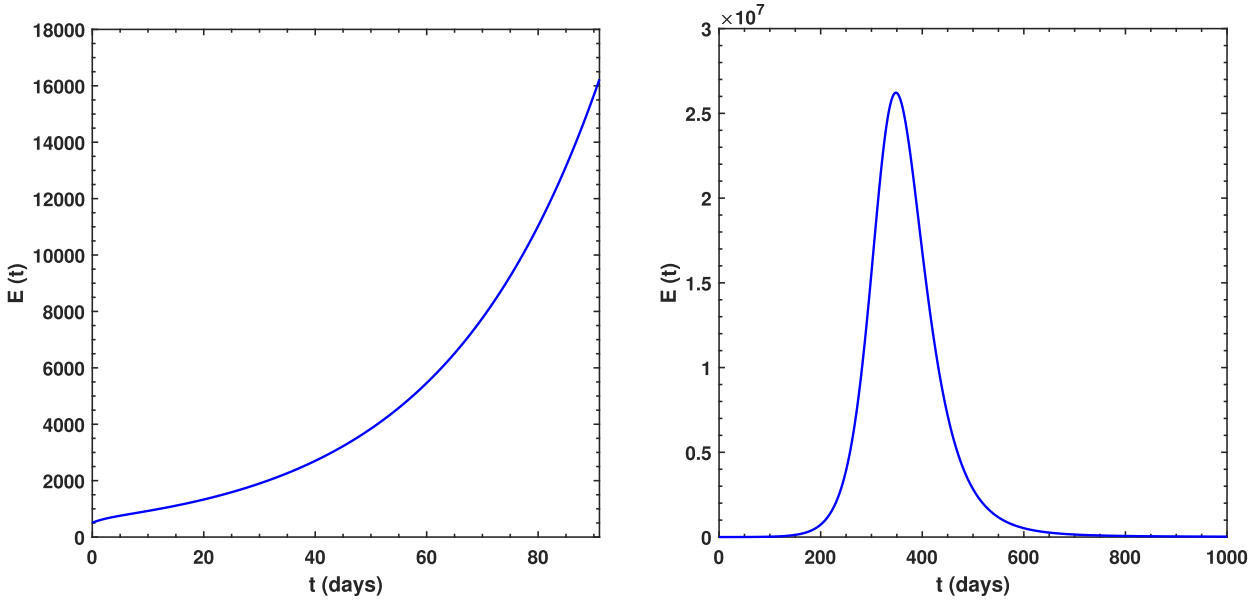


(a) (b)

**Fig. 7** **(a)** Behavior of exposed individuals for the time period $[0, 91]$ and **(b)** behavior of exposed individuals for the time period $[0, 1000]$ under the Caputo operator.

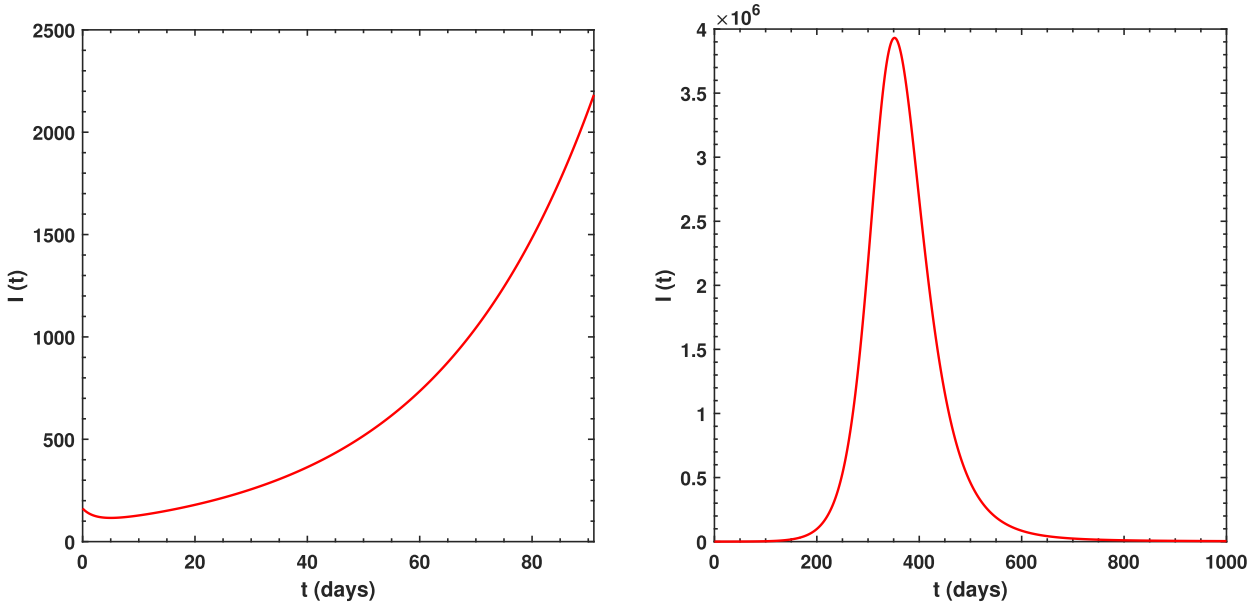


(a) (b)

**Fig. 8** **(a)** Behavior of infectious individuals for the time period $[0, 91]$ and **(b)** behavior of infectious individuals for the time period $[0, 1000]$ under the Caputo operator.

simulation consists of two plots for each class including the first one on a small interval of time whereas in the second plot considerably longer time period has been chosen to observe the dynamics of that particular class in future. Susceptible individuals seem to decline for the initial $16\frac{2}{3}$ months and later they start to improve by a slight amount whereas the exposed and the infectious class follow the symmetrical behavior with the bell-shaped curve depicting, once again, real behavior of any disease. As long as the hospitalized individuals are concerned, they sharply decline for about 6 months but later they also follow the bell-shaped structure. Last but not the least, the behavior of the dead and recovered

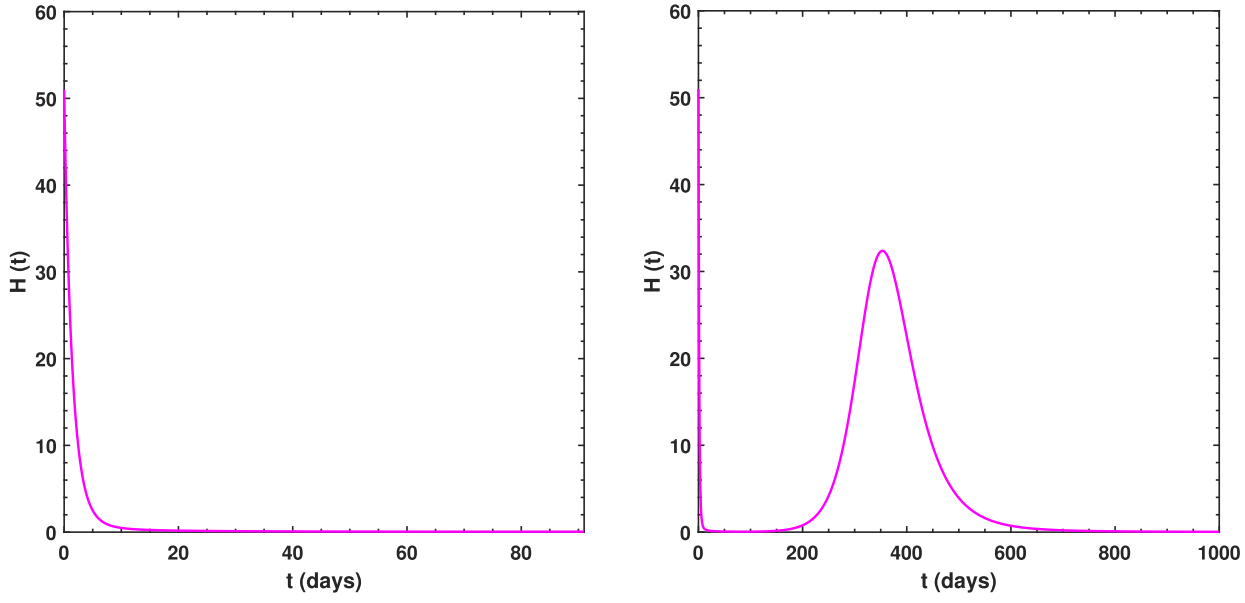


(a) (b)

**Fig. 9** **(a)** Behavior of hospitalized individuals for the time period $[0, 91]$ and **(b)** behavior of hospitalized individuals for the time period $[0, 1000]$ under the Caputo operator.

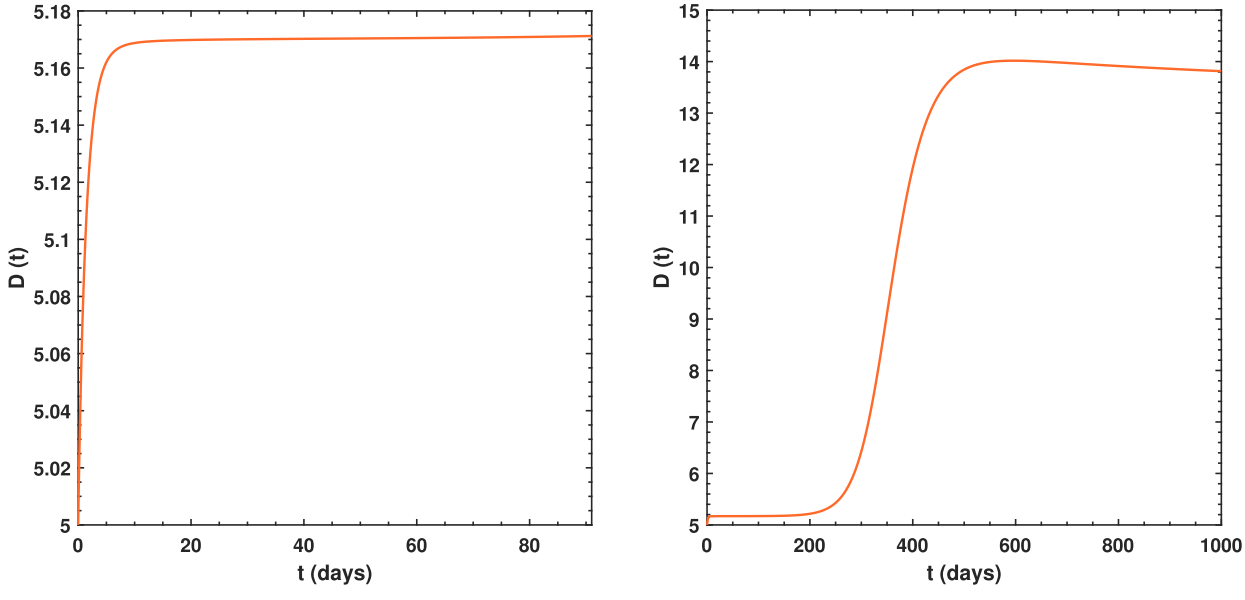


(a) (b)

**Fig. 10** **(a)** Behaviour of dead individuals for the time period $[0, 91]$ and **(b)** behaviour of dead individuals for the time period $[0, 1000]$ under the Caputo operator.

classes is shown in Figs. 10 and 11, respectively. There are not many people dead in this class as the infectious population decreases after about 16.5 months and as a result people start to have recovery as shown in the last figure. From all of this observation, it can be said that the COVID-19 epidemic is controllable provided that it may somehow be prevented from being spread from human to human by following measures and prevention imposed upon communities in the form of lockdown, hand-washing, covering the face and avoiding crowded places.

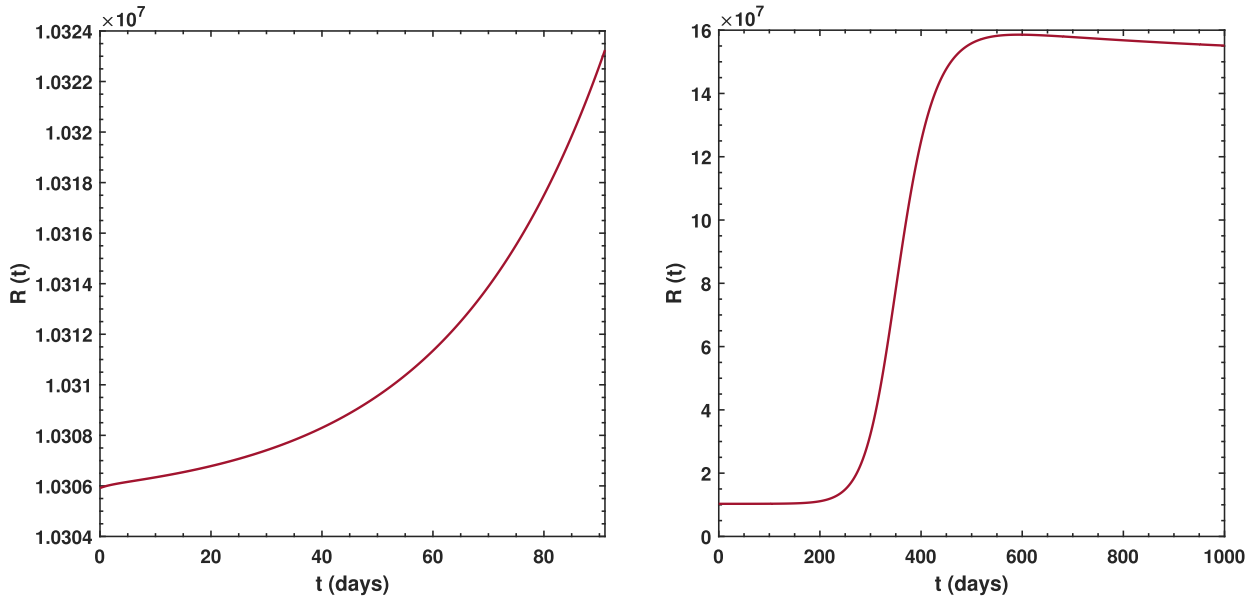


**Fig. 11** **(a)** Behaviour of recovered individuals for the time period $[0, 91]$ and **(b)** behaviour of recovered individuals for the time period $[0, 1000]$ under the Caputo operator.

## 6. CONCLUDING REMARKS

The Caputo-based model for increasing COVID-19 strains was investigated in this study. COVID-19 is one of the most dangerous and alarming diseases. The toxic effects of the COVID-19 pandemic are extremely fast-acting, and infection usually results in death within a few weeks. As a result, it is important to dig deeper into the dynamics of this subtle virus. In the literature, the fractional operator has been shown to be well-motivated in dealing with the transmission dynamics of infectious diseases. The fractionalized order in the study is $\alpha$, and the dimensional consistency between the other parameters was taken into account. As a consequence, some key aspects of the proposed fractional version of the model, such as model formation, existence and uniqueness of the solution through the fixed-point theorem, and stability analysis by means of UHS and GUHS, have been discussed. Moreover, under the least-squares method, fitted parameters of the model are obtained using actual occurrence cases of the virus and 3 months data points selected for the country of Nigeria. It must be noted that the data is arbitrarily taken from this country and any data maybe taken for validation of the proposed Caputo model.

By running simulations for both models, we were able to obtain the best-suited parameters, which are described in Table 4, noting that in addition to biological parameters, we were also able to obtain the optimized Caputo fractional-order parameter $\alpha$, which is approximately equal to $9.6481e-01$, while the minimum discrepancy observed in the classical and Caputo sense are $4.1543e+02$ and $4.0109e+02$, respectively. It can be observed that the Caputo results in the smaller error. It is worth noting that the fractional form of the SEIHDR model under investigation comprehends the disease's actions are better than the integer-order version. In addition, various numerical simulations were run using an effective numerical method to shed more light on the model's characteristics. Future research study of the Caputo model under consideration will be carried out with the optimal control theory under some control measures. This includes effective intervention strategies to curtail the spread of the infectious disease called the COVID-19.

## REFERENCES

1. F. Zhou *et al.*, Clinical course and risk factors for mortality of adult inpatients with COVID-19 in Wuhan, China: A retrospective cohort study, *Lancet* **395**(102) (2020) 1054–1062, https://doi.org/10.1016/S0140-6736(20)30566-3.
2. P. Wu *et al.*, Real-time tentative assessment of the epidemiological characteristics of novel coronavirus

infections in Wuhan, China, as at 22 January 2020, *Eurosurveillance* **25**(3) (2020) 2000044, https://doi.org/10.2807/1560-7917.ES.2020.25.3.2000044.

3. J. T. Wu, K. Leung and G. M. Leung, Nowcasting and forecasting the potential domestic and international spread of the 2019-nCoV outbreak originating in Wuhan, China: A modelling study, *Lancet* **395**(10225) (2020) 689–697, https://doi.org/10.1016/S0140-6736(20)30260-9.
4. S. Zhao *et al.*, Preliminary estimation of the basic reproduction number of novel coronavirus (2019-nCoV) in China, from 2019 to 2020: A data-driven analysis in the early phase of the outbreak, *Int. J. Infect. Dis.* **92** (2020) 214–217, https://doi.org/10.1016/j.ijid.2020.01.050.
5. N. Hamidreza and V. V. Kulish, Complexity-based classification of the coronavirus disease (COVID-19), *Fractals* **28**(5) (2020) 2050114, https://doi.org/10.1142/S0218348X20501145.
6. World Health Organization (WHO), Coronavirus Disease (COVID-19) Dashboard 2021, https://covid19.who.int.
7. Nigeria Center for Disease Control (NCDC). Coronavirus disease (COVID-19) pandemic 2021, https://covid19.ncdc.gov.ng.
8. Q. Li *et al.*, Early transmission dynamics in Wuhan, China, of novel coronavirus infected pneumonia, *New Engl. J. Med.* **382** (2020) 1199–1207, https://doi.org/10.1056/NEJMoa2001316.
9. Q. Ding, P. Lu, Y. Fan, Y. Xia and M. Liu, The clinical characteristics of pneumonia patients coinfected with 2019 novel coronavirus and influenza virus in Wuhan, *China J. Med. Virol.* **92**(9) (2020) 1549–1555, https://doi.org/10.1002/jmv.25781.
10. World Health Organization (WHO), Coronavirus disease (COVID-2019) pandemic 2021, https://www.who.int/emergencies/diseases/novel-coronavirus-2019.
11. S. Qureshi, Periodic dynamics of rubella epidemic under standard and fractional Caputo operator with real data from Pakistan, *Math. Comput. Simul.* **178** (2020), doi:10.1016/j.matcom.2020.06.002.
12. S. Qureshi and J. Rashid, Modeling of measles epidemic with optimized fractional order under Caputo differential operator, *Chaos Solitons Fractals* **145**(4) (2021) 110766.
13. N. H. Sweilam *et al.*, On the optimal control of coronavirus (2019-nCov) mathematical model; a numerical approach, *Adv. Differ. Equ.* **1** (2020) 528.
14. L.-L. Huang *et al.*, Discrete fractional calculus for interval-valued systems, *Fuzzy Sets Syst.* **404** (2021) 141–158.
15. M. M. Khader *et al.*, A spectral collocation method for solving fractional KdV and KdV–Burgers equations with non-singular kernel derivatives, *Appl. Numer. Math.* **161** (2021) 137–146
16. D. Baleanu and R. P. Agarwal, Fractional calculus in the sky, *Adv. Differ. Equ.* (2021) 117.
17. S. S. Musa, X. Wang, S. Zhao, S. Li, N. Hussaini, W. Wang and D. He, Heterogeneous severity of COVID-19 in African Countries: A modeling approach, doi:10.21203/rs.3.rs-426664/v1.
18. I. A. Baba, A. Yusuf, K. S. Nisar, A. H. Abdel-Aty and T. A. Nofal, Mathematical model to assess the imposition of lockdown during COVID-19 pandemic, *Res. Phys.* **20** (2021) 103716.
19. S. S. Musa, S. Qureshi, S. Zhao, A. Yusuf, U. T. Mustapha and D. He, Mathematical modeling of COVID-19 epidemic with effect of awareness programs, *Infect. Dis. Model.* **6** (2021) 448–460.
20. I. Ahmed, E. F. D. Goufo, A. Yusuf, P. Kumam, P. Chaipanya and K. Nonlaopon, An epidemic prediction from analysis of a combined HIV-COVID-19 coinfection model via ABC-fractional operator, *Alex. Eng. J.* **60**(3) (2021) 2979–2995.
21. Z. Memon, S. Qureshi and B. R. Memon, Assessing the role of quarantine and isolation as control strategies for COVID-19 outbreak: A case study, *Chaos Solitons Fractals* **144** (2021) 110655.
22. I. Ahmed, G. U. Modu, A. Yusuf, P. Kumam and I. Yusuf, A mathematical model of Coronavirus Disease (COVID-19) containing asymptomatic and symptomatic classes, *Res. Phys.* **21** (2021) 103776.
23. P. A. Naik, M. Yavuz, S. Qureshi, J. Zu and S. Townley, Modeling and analysis of COVID-19 epidemics with treatment in fractional derivatives using real data from Pakistan, *Eur. Phys. J. Plus* **135**(10) (2021) 1–42.
24. S. Rezapour, H. Mohammadi and M. E. Samei, SEIR epidemic model for COVID-19 transmission by Caputo derivative of fractional order, *Adv. Differ. Equ.* **2020**(1) (2020) 1–19.
25. Y. Zhang, X. Yu, H. Sun, G. R. Tick, W. Wei and B. Jin, Applicability of time fractional derivative models for simulating the dynamics and mitigation scenarios of COVID-19, *Chaos Solitons Fractals* **138** (2020) 109959.
26. D. He, S. Zhao, Q. Lin, S. S. Musa and L. Stone, New estimates of the Zika virus epidemic attack rate in Northeastern Brazil from 2015 to 2016: A modelling analysis based on Guillain–Barr Syndrome (GBS) surveillance data, *PLOS Negl. Trop. Dis.* **14**(4) (2020) 0007502.
27. S. S. Musa, S. Zhao, D. Gao, Q. Lin, G. Chowell and D. He, Mechanistic modelling of the large-scale Lassa fever epidemics in Nigeria from 2016 to 2019, *J. Theor. Biol.* **493** (2020) 110209.
28. S. Zhao, L. Stone, D. Gao and D. He, Modelling the large-scale yellow fever outbreak in Luanda, Angola, and the impact of vaccination, *PLOS Negl. Trop. Dis.* **12**(1) (2018) e0006158.

29. D. He, Y. Artzy-Randrup, S. S. Musa and L. Stone, The unexpected dynamics of COVID-19 in Manaus, Brazil: Herd immunity versus interventions, medRxiv (2021), https://doi.org/10.1101/2021.02.18.21251809.
30. N. H. Tuan, H. Mohammadi and S. Rezapour, A mathematical model for COVID-19 transmission by using the Caputo fractional derivative, *Chaos Solitons Fractals* **140** (2020) 110107.
31. A. Ali, F. S. Alshammari, S. Islam, M. A. Khan and S. Ullah, Modeling and analysis of the dynamics of novel coronavirus (COVID-19) with Caputo fractional derivative, *Res. Phys.* **20** (2021) 103669.
32. K. S. Nisar, S. Ahmad, A. Ullah, K. Shah, H. Alrabaiah and M. Arfan, Mathematical analysis of SIRD model of COVID-19 with Caputo fractional derivative based on real data, *Res. Phys.* **21** (2021) 103772.
33. I. Ahmed, I. A. Baba, A. Yusuf, P. Kumam and W. Kumam, Analysis of Caputo fractional-order model for COVID-19 with lockdown, *Adv. Differ. Equ.* **2020**(1) (2020) 1–14.
34. R. P. Yadav and R. Verma, A numerical simulation of fractional order mathematical modeling of COVID-19 disease in case of Wuhan China, *Chaos Solitons Fractals* **140** (2020) 110124.
35. M. Mohammad, A. Trounev and C. Cattani, The dynamics of COVID-19 in the UAE based on fractional derivative modeling using Riesz wavelets simulation, *Adv. Differ. Equ.* **2021**(1) (2021) 1–14.
36. H. Khan, Y. Li, A. Khan and A. Khan, Existence of solution for a fractional-order Lotka–Volterra reactiondiusion model with Mittag-Leffler kernel, *Math. Methods Appl. Sci.* **42**(9) (2019) 3377–3387.
37. H. Khan, T. Abdeljawad, M. Aslam, R. A. Khan and A. Khan, Existence of positive solution and HyersUlam stability for a nonlinear singular-delay-fractional differential equation, *Adv. Differ. Equ.* **2019** (2019) 104.
38. A. K. Tripathy, *Hyers–Ulam Stability of Ordinary Differential Equations* (Chapman and Hall/CRC, 2021).
39. K. Liu, M. Feckan and J. Wang, Hyers–Ulam stability and existence of solutions to the generalized Liouville–Caputo fractional differential equations, *Symmetry* **12** (2020) 955, doi:10.3390/sym12060955.
40. K. Diethelm, N. J. Ford and A. D. Freed, A predictor-corrector approach for the numerical solution of fractional differential equations, *Nonlinear Dyn.* **29**(1–4) (2002) 3–22.
41. K. Diethelm, N. J. Ford and A. D. Freed, Detailed error analysis for a fractional Adams method, *Numer. Algorithms* **36**(1) (2004) 31–52.
42. R. Almeida and S. Qureshi, A fractional measles model having monotonic real statistical data for constant transmission rate of the disease, *Fractal Fract.* **3**(4) (2019) 53.
43. H. W. Berhe, S. Qureshi and A. A. Shaikh, Deterministic modeling of dysentery diarrhea epidemic under fractional Caputo differential operator via real statistical analysis, *Chaos Solitons Fractals* **131** (2020) 109536.
44. S. Qureshi, Effects of vaccination on measles dynamics under fractional conformable derivative with Liouville–Caputo operator, *Eur. Phys. J. Plus* **135**(1) (2020) 63.
45. M. R. Mahmoudi, D. Baleanu, B. A. Tuan and K. H. Pho, A novel method to detect almost cyclostationary structure, *Alex. Eng. J.* **59**(4) (2020) 2339–2346.
46. S. Qureshi, Real life application of Caputo fractional derivative for measles epidemiological autonomous dynamical system, *Chaos Solitons Fractals* **134** (2020) 109744.
47. N. Anh Triet, V. Van Au, L. Dinh Long, D. Baleanu and N. Huy Tuan, Regularization of a terminal value problem for time fractional diffusion equation, *Math. Methods Appl. Sci.* **43**(6) (2020) 3850–3878.
48. R. Garrappa, Short tutorial: Solving fractional differential equations by Matlab codes, Department of Mathematics University of Bari, Italy (2014).